THE JOURNAL OF PHYSICAL CHEMISTRY Letters

Letter

Cite This: J. Phys. Chem. Lett. 2018, 9, 3392−3396

pubs.acs.org/JPCL

Diffraction-Detected Sum Frequency Generation: Novel Ultrafast X-ray Probe of Molecular Dynamics

Jérémy R. Rouxel,*,‡ Markus Kowalewski,*,‡ and Shaul Mukamel*

Department of Chemistry, University of California, Irvine, California 92697-2025, United States

Supporting Information

ABSTRACT: We propose a novel time-resolved diffraction technique based on sum frequency generation that combines an optical pump with an X-ray stimulated Raman probe. Simulations are presented for formyl fluoride, which is nonchiral in the ground state and evolves into a chiral nonplanar structure in the first excited state upon excitation by a circularly polarized UV pump. A coherently controlled elliptically polarized pump is used to prepare the molecule in a selected enantiomer and the chiral interconversion dynamics is then monitored by the probe diffraction.

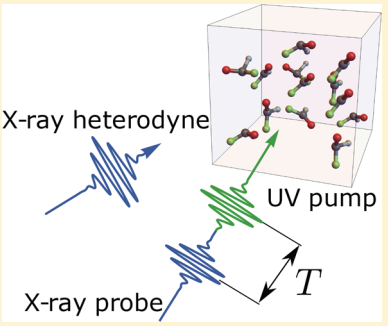

Sum frequency generation (SFG) spectroscopy is a second-order $\chi^{(2)}$ technique widely used to study vibrational dynamics of molecules at interfaces.[1−4] A single interaction with an infrared pulse first creates a vibrational coherence, and a broad-band visible pulse then generates the signal at a sum of the IR and visible frequencies, which is recorded as a function of the pulse delay (see Figure 1). We propose an X-ray extension of this technique, Figure 1a, which first uses a visible/UV pulse to create an electronic coherence, followed by a hard X-ray pulse that generates a diffraction signal at a sum of the UV and X-ray frequencies. In contrast to optical SFG, the scattering wavevector now provides a time-resolved diffraction image of the electronic coherence. Standard diffraction experiments detect the diagonal elements of the charge density operator that represent the charge density of a specific electronic state. The proposed experiment is made possible by recently developed ultrashort hard X-ray sources such as free electron laser (XFEL)[5,6] or synchrotron sources using the slicing scheme.[7] These new sources make ultrafast nonlinear X-ray spectroscopy[8,9] and diffraction[10−15] a reality. While such sources can induce significant photodamage in the sample, the combination of a diffract-before-destroy detection strategy and the use of a jet sample injector allow one to disregard this issue.[16]

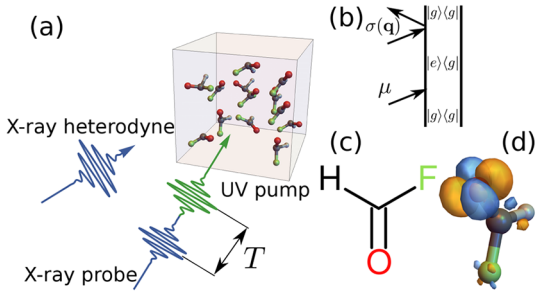

Figure 1. (a) SFG experimental setup. Excited-state dynamics is launched by a UV pump pulse, and after a delay T, an X-ray pulse is diffracted by an ensemble of randomly oriented molecules. (b) Diagram representing the stimulated SFG signal, eq 2. (c) Lewis structure of formyl fluoride. (d) Transition charge density between the ground and first excited states for the planar configuration.

In previous work,[17] we simulated the SFG diffraction signal from an oriented formyl fluoride and demonstrated that this technique can image time-evolving transition current densities. Here, we extend that study in three ways. First, we consider a randomly oriented sample of formyl fluoride, Figure 1c. Second, we include nuclear dynamics. As a consequence of rotational averaging, the diffraction is dominated by the one-molecule contribution that scales with the number of scatterers and exhibits ring patterns.[18] This planar and achiral molecule in its ground state (Figure 1c,d) has an excited-state double-well potential along the out-of-plane stretching mode, which represents two nonplanar enantiomers that interconvert on a femtosecond time scale. Third, we use a coherent control scheme to shape the elliptically polarized pump pulse in order to prepare a nuclear wave packet initially localized at one selected enantiomer, Figure 2. Diffraction of the subsequent X-ray pulse can then image the chiral dynamics. The technique should further provide a sensitive probe for coupled electronic and vibrational dynamics during the delay period, including nonadiabatic processes and conical intersections. These go beyond the present study.

Received: April 9, 2018
Accepted: June 4, 2018
Published: June 4, 2018

DOI: 10.1021/acs.jpclett.8b01095
J. Phys. Chem. Lett. 2018, 9, 3392−3396

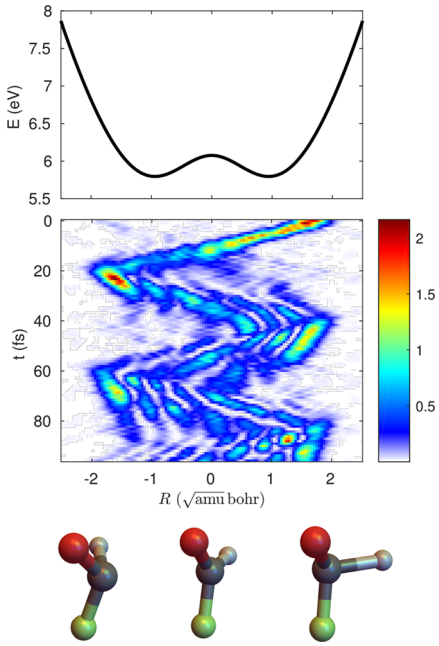

Figure 2. Enantiomeric interconversion dynamics in formyl fluoride after interaction with an elliptically polarized shaped pump pulse that selects a single enantiomer. R is the out-of-plane bending nuclear coordinates of the molecule. Upper panel: first excited-state potential. Lower panel: time evolution of the nuclear wave packet in the electronic excited state ($|\Psi_e(t)|^2$) following the pump pulse excitation. The molecular configurations corresponding to the normal coordinates are shown at the bottom. Time slices of the nuclear dynamics are shown in the Supporting Information, Figure S3.

We first define the time-resolved stimulated diffraction signal. The numerical approach and the computed signals are then presented and followed by a conclusion.

When the X-ray pulse is off-resonant with respect to core excitations, its diffraction may be described by the minimal coupling Hamiltonian for the radiation−matter interaction[19,20]

$$H_{\text{int}}(t) = \frac{e}{2mc}\int \mathrm{d}\mathbf{r}\, \sigma(\mathbf{r})\mathbf{A}^2(\mathbf{r}, t) \tag{1}$$

where $\sigma(\mathbf{r})$ is the charge density operator and $\mathbf{A}(\mathbf{r},t)$ is the vector potential of the field.

Time-resolved diffraction signals can be measured either by the spontaneous (homodyne) or by the stimulated (heterodyne) detection mode. The spontaneous two-molecule signal vanishes in isotropic, nonchiral samples, which lack long-range order.[18] A stimulated signal is generated by interaction with two fields $\mathbf{A}_{\text{XR}}(t)$ and $\mathbf{A}_{\text{het}}(t)$.[17] $\mathbf{A}_{\text{XR}}(t)$ creates the diffracted field, which interferes with $\mathbf{A}_{\text{het}}(t)$, and the resulting phase detection of X-ray diffraction resolves the phase problem.[21]

We will calculate the time-resolved chiral diffraction signal initiated by a UV pulse. To first order in that pulse, the rotationally averaged signal depicted in Figure 1b is given by

$$S_{\text{stim}}(\mathbf{q}, T) = 2N\Im \int \mathrm{d}t\, \mathrm{d}t_1\, \mathbf{A}^*_{\text{het}}(t)\cdot\mathbf{A}_{\text{XR}}(t)\mathbf{A}_{\text{pump}}(t - t_1 + T) \times \langle\sigma(\mathbf{q}, t)\boldsymbol{\mu}(t_1)\rangle_\Omega \tag{2}$$

where $\mathbf{q}$ is the scattering wavevector and $\boldsymbol{\mu} = \int \mathrm{d}\mathbf{r}\, \mathbf{j}(\mathbf{r})$ is the space-integrated current density operator, which gives the electric dipole operator in the momentum representation, and Ω stands for rotational averaging by integration over a sphere. $\mathbf{A}_{\text{XR}}(t)$ is the incoming diffracted X-ray pulse, and $\mathbf{A}_{\text{het}}(t)$ is the detected heterodyne pulse. When a single interaction with the pump creates a coherence between the ground g and the first excited e states, eq 2 can be recast as[17]

$$S_{\text{stim}}(\mathbf{q}, T) = 2N\Im f_{eg}(T)\langle\sigma_{ge}(\mathbf{q})\boldsymbol{\epsilon}_{\text{pump}}\cdot\boldsymbol{\mu}_{eg}\rangle_\Omega \tag{3}$$

where $\boldsymbol{\epsilon}_{\text{pump}}$ is the pump pulse polarization and the line shape function $f_{eg}(T)$ is given in the Supporting Information. The commonly used homodyne detection signal, in contrast, depends on $|\sigma_{ge}(\mathbf{q})|^2$[17] rather than $\sigma_{ge}(\mathbf{q})$. The transition charge density $\sigma_{ge}(\mathbf{q})$ is given by

$$\sigma_{ge}(\mathbf{q}) = N\int \mathrm{d}\mathbf{r}_1 \ldots \mathrm{d}\mathbf{r}_N\, \mathrm{e}^{-i\mathbf{q}\cdot\mathbf{r}_1}\Psi_g(\mathbf{r}_1 \ldots \mathbf{r}_N)\Psi^*_e(\mathbf{r}_1 \ldots \mathbf{r}_N) \tag{4}$$

where $\Psi_g(\mathbf{r})$ and $\Psi_e(\mathbf{r})$ are the ground- and first excited-state wave functions of the molecule. A real space movie of the evolving charge density is obtained by the Fourier transform

$$S_{\text{stim}}(\mathbf{r}, T) = \int \mathrm{d}\mathbf{q}\, \mathrm{e}^{i\mathbf{q}\cdot\mathbf{r}}S_{\text{stim}}(\mathbf{q}, T) \tag{5}$$

Formyl fluoride (Figure 1) is planar in its electronic ground state and assumes two enantiomeric chiral structures generated by out-of-plane bending in its first electronic excited state S_1. To obtain clear enantiomeric conversion dynamics, we need to prepare a photoexcited molecule initially in a single enantiomer. We used an optimal control pulse shaping strategy[22,23] for the elliptically polarized pump to create a localized wave packet in the first electronic state. The x and y components of the electric field were controlled independently. The control mechanism is based on the fact that both components of the pump laser field can interact with transition dipole moments of different parity with respect to the nuclear motion. Starting with an even ground state, the x component of the field interacts with an even transition dipole to create the even wave function in the excited state. The y field component interacts with an odd transition dipole moment, creating an odd excited-state wave function. A proper superposition of the even and odd nuclear wave packets results in an enantiomeric excess, i.e., a wave packet localized in one potential well. We have used an optimal control protocol to independently optimize the x and y components. Details of the optimal control protocol and the optimized shaped pump pulse are given in the Supporting Information. The resulting wave wave packet, created by the elliptically polarized pump pulse, is shown in the middle panel of Figure 2.

Our coherent control target is to optimize the elliptically polarized pump in order to create an excited-state wave packet localized at a single enantiomer. The Hamiltonian of the molecular system is given by

$$H_0 = -\frac{1}{2m}\frac{\mathrm{d}}{\mathrm{d}R} + \hat{V}_g(R) + \hat{V}_e(R) \tag{6}$$

where R is the mass-weighted normal-mode displacement, m = 1822 is the reduced mass of the normal mode (in atomic units), and $\hat{V}_g$ and $\hat{V}_e$ are the potential energy curves of the electronic ground state and the first electronic excited state, respectively. To prepare the molecule in a desired chiral state, we employ an elliptically polarized pump pulse propagating along the z direction. The interaction with the pump pulse is $H_{\text{int}} = \boldsymbol{\mu}(R)\cdot\mathbf{E}_{\text{pu}}(t)$, where $\boldsymbol{\mu}$ is the transition dipole moment shown in the Supporting Information. To address target states of different symmetry, we use components of $\boldsymbol{\mu}$ that are of odd and even in the vibrational mode. The time evolution of the

DOI: 10.1021/acs.jpclett.8b01095
J. Phys. Chem. Lett. 2018, 9, 3392−3396

initial wave packet, governed by $H_0 + H_{int}$, is calculated by the Chebyshev propagation scheme.[24]

A localized and displaced wave packet (see Figure 2) in the electronic excited state is generated by using optimal control theory (OCT) to determine a pump laser field. We use an OCT approach based on the Krotov method.[25,26] The control functional reads

$$J[\Psi_f(t), \Psi_i(t), E_i(t)] = |\langle\Psi_i(T)|\Phi_f\rangle|^2 - \alpha_0 \int_0^T dt\, \frac{|E_i(t) - \tilde{E}_i(t)|^2}{s(t)} - 2\Re\left[\langle\Psi_i(T)|\Phi_f\rangle \int_0^T dt\, \langle\Psi_f(t)|i(H_0 + H_{int}) + \frac{\partial}{\partial t}|\Psi_i(t)\rangle\right] \quad (7)$$

where Ψ_i is the initial wave function and T the final time of the propagation. Here $\Psi_i(t = 0)$ is defined as the as the vibrational ground state of the electronic ground states. The target wave function Φ_f is set as a Gaussian with a width of 0.39 au (fwhm) centered at 1.7 au, which corresponds to one of the enantiomers. The Krotov change parameter α_0 is set to 1, and the shape function $s(t) = \sin(t\pi/T)^2$ guarantees smooth on and off switching of the laser field. The iterative solution of the optimization procedure[25] yields a time-discretized field $E_i(t)$, i.e., one of the two components (x or y) of the elliptically polarized laser field. To achieve a total field with balanced x and y components, the iteration procedure alternates between both components (8 steps for x, 8 steps for y, 20 steps for x, 20 steps for y). First a solution for $E_x(t)$ is calculated with a fixed field $E_y(t)$ from a previous optimization (or an initial guess), and after that a solution for $E_y(t)$ is calculated by using the previously calculated field as a fixed field $E_x(t)$. This procedure yielded a wave packet that has a 86% overlap with the target wave function. The optimized electric fields in the time and the frequency domains are shown in Figure 3. The enantiomeric excess optimization has been carried out on an oriented molecule. Subsequent random averaging needs to be achieved, leading to a 1/3 factor that decreases the yield substantially.[27] The rotational averaging does not destroy the creation of an enantiomeric excess because it is the angular momentum of the light, independent of the relative molecular orientation, that drives the chiral dynamics. As of today, an experimental realization of an efficient coherent control scheme of molecular chirality has still not been demonstrated.[28−30]

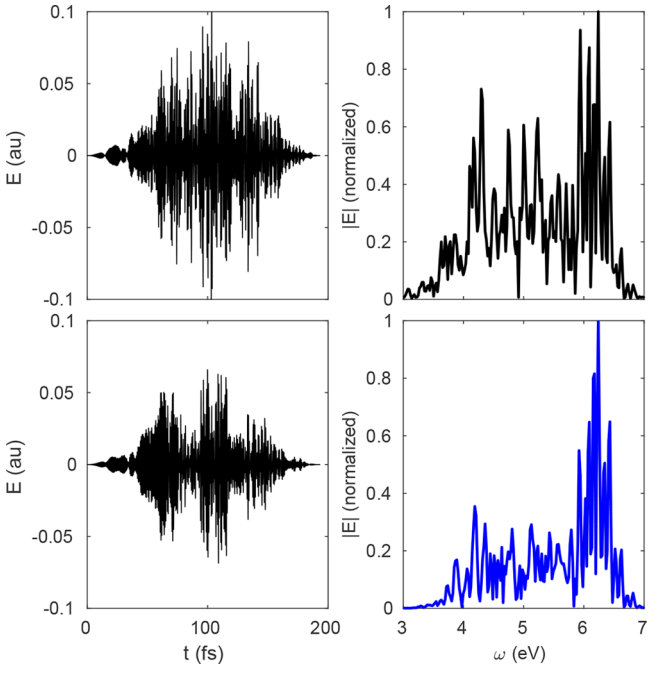

Figure 3. Components of the elliptical polarized pump field that create the localized wave packet. The left column shows the electric fields in the time domain, and the right column shows the electric fields in the frequency domain. The upper and lower rows are the x and the y components, respectively.

Upon interacting with the pump, the free molecule interconverts between the two enantiomers, as shown in the other panels of Figure 2, until after a delay T when it is finally probed by the diffraction of an X-ray probe pulse.

The diffraction signal monitors the wave packet evolution in the excited state. Snapshots of the animation of the time-resolved SFG X-ray diffraction signal and dynamics given in Supporting Information are displayed in Figure 4. The

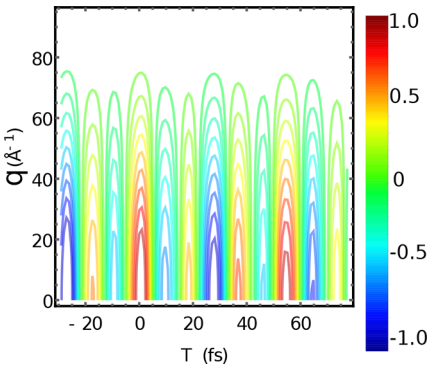

Figure 4. Orientationally averaged stimulated X-ray SFG signal $S_{stim}(\mathbf{q},T)$, eq 3 vs the delay times T. In an isotropic sample, the signal has a radial symmetry and thus only depends on the norm of $\mathbf{q}$.

diffracted X-ray pulse $\mathbf{A}_{XR}$ (see eq 2) and the heterodyning pulse $\mathbf{A}_{het}$ are 5 fs long. The signal shows a 23 fs oscillatory period corresponding to the enantiomeric interconversion.

A Fourier transform of eq 5 to real space, as defined in the Supporting Information, generates the signal displayed in Figure 5. The real space signal reveals the rotationally averaged off-diagonal matrix element of the charge density. This signal from an oriented sample[17] can reveal an image of the transition charge density (Figure 1d). In Figure 5, the coherent control pulse interacts with the matter in order to prepare a localized wave packet in a single enantiomer at time zero (see Figure 2). After this, the system can freely evolve for a delay T, and we observe oscillations in the signal that correspond to the wave packet moving back and forth between the two enantiomeric minima as visible in the signal defined in q space. The measured $\mathbf{r}$ dependence provides the rotationally averaged transition charge density $\langle\sigma_{eg}(r)\rangle_\Omega$. While structural details are lost in the rotational averaging, the signal still offers information on the displacement length of the electronic cloud induced by this transition. We see that the X-ray diffraction signals in the liquid phase or in crystals are widely used to probe long-range order in matter because the homodyne signals that originate from pairs of molecules vanish in an isotropic sample. We have shown that stimulated or spontaneous X-ray signals originating from a single molecule in an isotropic sample can nevertheless provide valuable information. Measurements are simpler in ensembles of randomly oriented molecules, but orientational averaging of the matter correlation function makes it impossible to recover the complete molecular structure. Combined with

DOI: 10.1021/acs.jpclett.8b01095
J. Phys. Chem. Lett. 2018, 9, 3392−3396

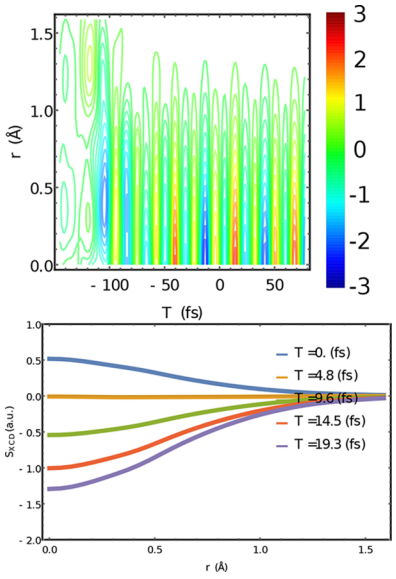

Figure 5. Top: orientationally averaged stimulated X-ray SFG signal $S_{stim}(\mathbf{r},T)$, eq 5 vs the delay times T. The shaped pulse induces the dynamics displayed in Figure 2, and the pump ends at T = 0 fs. Bottom: slices of the signals are various times.

the emerging ultrafast capabilities of X-ray pulses, SFG X-ray diffraction offers a new window into the excited-state dynamics in molecules. Typical incoming energies for X-ray diffraction are near 10 keV. The detector resolution has to have good frequency resolution at these energies in order to separate the inelastic signal of interest. While a difficult task, this is now possible; for example, the swissFEL PSSS detector (photon single shot spectrometer) can measure spectra with a resolution of $\Delta E/E = (2-5) \times 10^{-5}$ in the 4−12 keV range. In our case, the needed energy resolution is (5 eV)/(10 keV) = 0.0005 and is 1 order of magnitude larger that the detector limit.[31] We have employed the SFG signal to follow in real time the enantiomeric dynamics in formyl fluoride, and it complements the time-resolved CD signal.[32]

When using the multipolar Hamiltonian, the electric and the magnetic dipoles have a well-defined parity, and one can easily find out which contribution appears at a given order in the multipolar expansion. The charge density matrix elements constitute scalar fields that need not be eigenvalues of the parity operator $\mathcal{P}$ (defined by $\mathcal{P}\sigma(\mathbf{r}) = \sigma(-\mathbf{r})$). They can be decomposed into symmetric and antisymmetric components $\sigma(\mathbf{r}) = \sigma_s(\mathbf{r}) + \sigma_{as}(\mathbf{r})$, where $\sigma_{as}(\mathbf{r}) = \frac{1}{2}(\sigma(\mathbf{r}) - \sigma(-\mathbf{r}))$ and $\sigma_s(\mathbf{r}) = \frac{1}{2}(\sigma(\mathbf{r}) + \sigma(-\mathbf{r}))$. It follows that $\mathcal{P}\sigma_{as}(\mathbf{r}) = -\sigma_{as}(\mathbf{r})$ and $\mathcal{P}\sigma_s(\mathbf{r}) = \sigma_s(\mathbf{r})$. In a nonchiral molecule, $\langle\sigma_{as}\rangle_\Omega = 0$, while in a chiral molecule, both $\langle\sigma_s\rangle_\Omega$ and $\langle\sigma_{as}\rangle_\Omega$ are nonzero. Then, the time-resolved diffraction signal on a randomly oriented sample measures only $\langle\sigma_s\rangle_\Omega$ when the molecule is nonchiral and the total charge density when it is chiral. Designing a chiral signal that could selectively probe $\langle\sigma_{as}\rangle_\Omega$ and vanishes for nonchiral molecules is an open challenge.

■ ASSOCIATED CONTENT

Supporting Information

The Supporting Information is available free of charge on the ACS Publications website at DOI: 10.1021/acs.jpclett.8b01095.

Extra information on the averaging scheme, the line shape function, and the quantum chemistry calculations (PDF)

■ AUTHOR INFORMATION

Corresponding Authors

*E-mail: jrouxel@uci.edu (J.R.R.).
*E-mail: mkowalew@uci.edu (M.K.).
*E-mail: smukamel@uci.edu (S.K.).

ORCID

Jérémy R. Rouxel: 0000-0003-3438-6370
Markus Kowalewski: 0000-0002-2288-2548
Shaul Mukamel: 0000-0002-6015-3135

Author Contributions

‡J.R.R. and M.K. contributed equally.

Notes

The authors declare no competing financial interest.

■ ACKNOWLEDGMENTS

The support of the Chemical Sciences, Geosciences, and Biosciences division, Office of Basic Energy Sciences, Office of Science, U.S. Deparment of Energy through Award No. DE-FG02-04ER15571 and of the National Science Foundation (Grant No. CHE-1663822) is gratefully acknowledged. J.R.R. was supported by the DOE grant.

■ REFERENCES

(1) Shen, Y. Surface properties probed by second-harmonic and sum-frequency generation. *Nature* **1989**, *337*, 519−525.
(2) Nagata, Y.; Mukamel, S. Vibrational sum-frequency generation spectroscopy at the water/lipid interface: molecular dynamics simulation study. *J. Am. Chem. Soc.* **2010**, *132*, 6434−6442.
(3) Hsieh, C.-S.; Okuno, M.; Hunger, J.; Backus, E. H.; Nagata, Y.; Bonn, M. Aqueous Heterogeneity at the Air/Water Interface Revealed by 2D-HD-SFG Spectroscopy. *Angew. Chem., Int. Ed.* **2014**, *53*, 8146−8149.
(4) Stiopkin, I. V.; Jayathilake, H. D.; Bordenyuk, A. N.; Benderskii, A. V. Heterodyne-detected vibrational sum frequency generation spectroscopy. *J. Am. Chem. Soc.* **2008**, *130*, 2271−2275.
(5) Ding, Y.; Huang, Z.; Ratner, D.; Bucksbaum, P.; Merdji, H. Generation of attosecond x-ray pulses with a multicycle two-color enhanced self-amplified spontaneous emission scheme. *Phys. Rev. Spec. Top.–Accel. Beams* **2009**, *12*, 060703.
(6) Chini, M.; Zhao, K.; Chang, Z. The generation, characterization and applications of broadband isolated attosecond pulses. *Nat. Photonics* **2014**, *8*, 178.
(7) Khan, S.; Holldack, K.; Kachel, T.; Mitzner, R.; Quast, T. Femtosecond undulator radiation from sliced electron bunches. *Phys. Rev. Lett.* **2006**, *97*, 074801.
(8) Chergui, M.; Collet, E. Photoinduced Structural Dynamics of Molecular Systems Mapped by Time-Resolved X-ray Methods. *Chem. Rev.* **2017**, *117*, 11025−11065.
(9) Chen, L.; Zhang, X.; Shelby, M. Recent advances on ultrafast X-ray spectroscopy in the chemical sciences. *Chemical Science* **2014**, *5*, 4136−4152.
(10) Kupper, J.; et al. X-ray diffraction from isolated and strongly aligned gas-phase molecules with a free-electron laser. *Phys. Rev. Lett.* **2014**, *112*, 083002.
(11) Kupitz, C.; et al. Serial time-resolved crystallography of photosystem II using a femtosecond X-ray laser. *Nature* **2014**, *513*, 261.
(12) Biggs, J. D.; Zhang, Y.; Healion, D.; Mukamel, S. Two-dimensional stimulated resonance Raman spectroscopy of molecules with broadband X-ray pulses. *J. Chem. Phys.* **2012**, *136*, 174117.

DOI: 10.1021/acs.jpclett.8b01095
J. Phys. Chem. Lett. 2018, 9, 3392−3396

(13) Zhang, Y.; Biggs, J. D.; Mukamel, S. Understanding excitation energy transfer in metalloporphyrin heterodimers with different linkers, bonding structures, and geometries through stimulated X-ray Raman spectroscopy. *J. Mod. Opt.* **2014**, *61*, 558−567.
(14) Son, S.-K.; Chapman, H. N.; Santra, R. Determination of multiwavelength anomalous diffraction coefficients at high x-ray intensity. *J. Phys. B: At., Mol. Opt. Phys.* **2013**, *46*, 164015.
(15) Tamasaku, K.; Shigemasa, E.; Inubushi, Y.; Katayama, T.; Sawada, K.; Yumoto, H.; Ohashi, H.; Mimura, H.; Yabashi, M.; Yamauchi, K.; Ishikawa, T. X-ray two-photon absorption competing against single and sequential multiphoton processes. *Nat. Photonics* **2014**, *8*, 313.
(16) Wang, D.; Weierstall, U.; Pollack, L.; Spence, J. Double-focusing mixing jet for XFEL study of chemical kinetics. *J. Synchrotron Radiat.* **2014**, *21*, 1364−1366.
(17) Rouxel, J. R.; Kowalewski, M.; Bennett, K.; Mukamel, S. Direct X-Ray sum frequency generation imaging of ultrafast electron dynamics. *arXiv:1802.04421***2018**.
(18) Stewart, G. X-ray diffraction in liquids. *Rev. Mod. Phys.* **1930**, *2*, 116.
(19) Salam, A. In *Molecular Quantum Electrodynamics: Long-Range Intermolecular Interactions*; Wiley, 2009; DOI: 10.1002/9780470535462
(20) Suryanarayana, C.; Norton, M. G. *X-ray diffraction: a practical approach*; Springer Science & Business Media, 2013.
(21) Schülke, W. *Electron dynamics by inelastic X-ray scattering*; Oxford University Press, 2007; Vol. 7.
(22) Zhu, W.; Botina, J.; Rabitz, H. Rapidly convergent iteration methods for quantum optimal control of population. *J. Chem. Phys.* **1998**, *108*, 1953−1963.
(23) Shi, S.; Rabitz, H. Quantum mechanical optimal control of physical observables in microsystems. *J. Chem. Phys.* **1990**, *92*, 364−376.
(24) Tal-Ezer, H.; Kosloff, R. An accurate and efficient scheme for propagating the time dependent Schrödinger equation. *J. Chem. Phys.* **1984**, *81*, 3967−3971.
(25) Somlói, J.; Kazakov, V. A.; Tannor, D. J. Controlled dissociation of I2 via optical transitions between the X and B electronic states. *Chem. Phys.* **1993**, *172*, 85−98.
(26) von den Hoff, P.; Thallmair, S.; Kowalewski, M.; Siemering, R.; de Vivie-Riedle, R. Optimal control theory - closing the gap between theory and experiment. *Phys. Chem. Chem. Phys.* **2012**, *14*, 14460.
(27) Shao, J.; Hänggi, P. Control of molecular chirality. *J. Chem. Phys.* **1997**, *107*, 9935−9941.
(28) Hoki, K.; González, L.; Fujimura, Y. Quantum control of molecular handedness in a randomly oriented racemic mixture using three polarization components of electric fields. *J. Chem. Phys.* **2002**, *116*, 8799−8802.
(29) Misawa, K. Applications of polarization-shaped femtosecond laser pulses. *Advances in Physics: X* **2016**, *1*, 544−569.
(30) Zhdanov, D. V.; Zadkov, V. N. Absolute asymmetric synthesis from an isotropic racemic mixture of chiral molecules with the help of their laser orientation-dependent selection. *J. Chem. Phys.* **2007**, *127*, 244312.
(31) Rehanek, J.; et al. The hard X-ray Photon Single-Shot Spectrometer of SwissFELinitial characterization. *J. Instrum.* **2017**, *12*, P05024.
(32) Rouxel, J. R.; Kowalewski, M.; Mukamel, S. Photoinduced molecular chirality probed by ultrafast resonant X-ray spectroscopy. *Struct. Dyn.* **2017**, *4*, 044006.

DOI: 10.1021/acs.jpclett.8b01095
J. Phys. Chem. Lett. 2018, 9, 3392−3396